Vibration Suppression Method using Disturbance Observer in Sensorless 120-degree Conduction Compressor Motor Drive

Yusuke Omi*, Takumi Yasuda*, Hirotaka Kato*, Hiroki Watanabe*, and Jun-ichi Itoh*
* Nagaoka University of Technology,
1603-1, Kamitomioka-cho, Nagaoka-shi, Niigata, 940-2188, Japan

***Abstract*--This paper proposes a vibration suppression method for a compressor motor driven in the sensorless 120-degree conduction mode. The proposed method estimates motor speed and angle by zero-crossing points of back EMF and suppresses vibration using a disturbance observer in conjunction with a Smith compensator. The experimental results demonstrate that the proposed method reduces the fundamental frequency component of vibration by 94.2% at a low speed of 15 rps (0.19p.u.).**

***Index Terms*— Compressor, Disturbance observer, IPMSM, 120-degree conduction mode.**

I. INTRODUCTION

Home applications, such as air conditioners and refrigerators, are required to be not only compact and highly efficient but also operate with minimal acoustic noise and vibration. These home appliances utilize a compressor in order to achieve a high-pressure refrigerant. The compressor operates through the cycle of (1) suction, (2) compression, and (3) discharge for heat exchange. This repetitive operation causes load torque fluctuations and motor speed ripple. Besides, the motor is enclosed within the compressor housing. In addition, speed sensors and position sensors cannot be attached to the motor because the inside of the compressor case is high temperature and pressure.

Interior Permanent Magnetic Synchronous Motors (IPMSMs) are widely utilized for compressor drive systems in home appliances thanks to their distinct advantages of high power density and high efficiency [1-4]. A vibration reduction method based on a position sensorless control for the IPMSM, leveraging Fourier transform and repetitive control, has been previously introduced [5]. The estimated load torque variation is compensated using a simplified Fourier transform and its inverse in [6]. However, these methods control the current in a rotating reference frame and require complex computations for the sensorless vector control (Field orient control), including the coordinate transformations. In addition, these methods based on sensorless vector control are challenging in maintaining accurate speed control when motor parameters change.

In order to solve these problems, the authors have proposed a vibration reduction method that employs an instantaneous current control and feedforward current command for the compressor driven in the sensorless 120-degree conduction mode [7]. In the sensorless 120-degree conduction mode, the rotor position and motor speed are estimated from the zero-crossing points (ZCPs) of back EMF, detected at every 60 electrical degrees [8]. Consequently, the sensorless 120-degree conduction mode is highly robust to motor parameter variations in terms of speed detection [9]. In Ref. [7], the current command that suppresses the vibration is derived from the known load torque characteristics. Additionally, compressor vibrations are reduced by a current control based on the mechanical angle that is estimated off-line. However, this control strategy is limited to operating the expected motor speed and load torque characteristics.

This paper proposes a vibration suppression method using a disturbance observer for a compressor driven in the sensorless 120-degree conduction mode. The proposed method estimates the load torque from the current command and the estimated speed, obtained at every 60 electrical degrees, using a disturbance observer. Thus, the proposed control method eliminates the necessity for the load torque characteristics in vibration suppression. In the sensorless 120-degree conduction mode, the average speed is estimated from the time interval between the detection times of two ZCPs, corresponding to every 60 electrical degrees. This indicates that the estimated speed ω_{es} has a dead time of 60 electrical degrees with respect to the true speed. The dead time deteriorates the stability of the control system. Therefore, the proposed method applies a Smith compensator with the disturbance observer in order to improve the stability. The effect of the dead time is canceled in the transfer function of the proposed system.

This paper is organized as follows; first, the load characteristics of a compressor subjected to this paper are described; next, the drive system for the compressor drive motor is described; moreover, the proposed vibration suppression method is explained; at last, the proposed method is verified by experiments using the compressor.

II. Drive System For Compressor Drive Motor

A. Load torque Characteristics of compressor

Fig. 1 shows the load torque characteristics of a reciprocating compressor subject to this paper. The reciprocating compressor periodically switches three processes: (1) the suction, (2) the compression, and (3) the ejection during the rotation of the rotor. As a result, the load torque characteristic of the compressor fluctuates in one period of the mechanical angle. It has been pointed out that the load torque characteristic is determined by the discharge pressure and suction pressure of the refrigerant in the compressor [10].

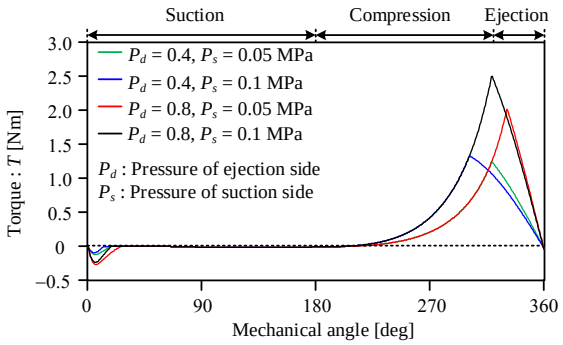

Fig. 1. Load torque characteristics.

B. Sensorless 120-degree conduction mode

Fig. 2 shows a conceptual diagram of the 120-degree conduction mode. The voltage is applied to two of three phases corresponding to the estimated electrical angle, and the phases in conduction are switched every 60 electrical degrees. The current is controlled by adjusting the output voltage with PWM. The control current i_{ad} is defined as the average of the currents of the two conduction phases. The electrical angle is estimated by detecting the ZCPs. The ZCPs are detected during the open interval of each phase. The motor speed is estimated from the time interval between two detected ZCPs.

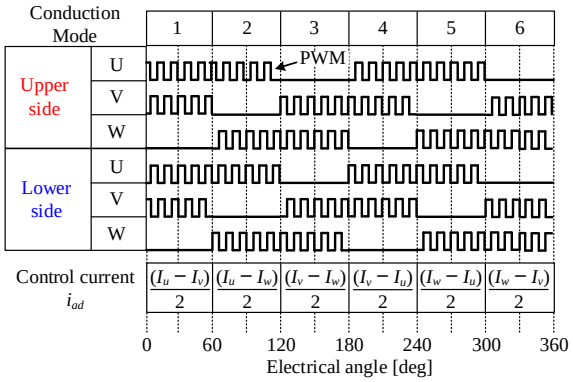

Fig. 2. Conceptual diagram of 120-degree conduction mode.

In the sensorless 120-degree conduction mode, the conduction phase is switched every 60 electrical degrees. During the switching period of the conduction phase (commutation period), the current in the conduction phase decreases to zero, leading to a change in the mode from the conducting state to the open state. If the ZCPs occur before the current value is zero during the commutation period, the motor speed is not estimated. This is because the open phase conducts to the power supply or GND during the commutation period so that the back EMF is not detected. Therefore, in this paper, the phase advance angle control is applied [11]. The phase advance control increases the time between changing the conduction phase and ZCP detection. Thus, the ZCPs are detected even when the commutation period is long. In this paper, the advance angle value is set to 30 degrees to ensure the detection of the ZCPs.

C. Control strategy of motor drive system

Fig. 3 shows the control block diagram for the compressor drive motor using the 120-degree conduction mode. Fig. 4 shows the circuit diagram of the three-phase inverter. The control block diagram mainly comprises a current control (ACR) and speed control (ASR). The ACR consists of a PI controller, which outputs the duty ratio of

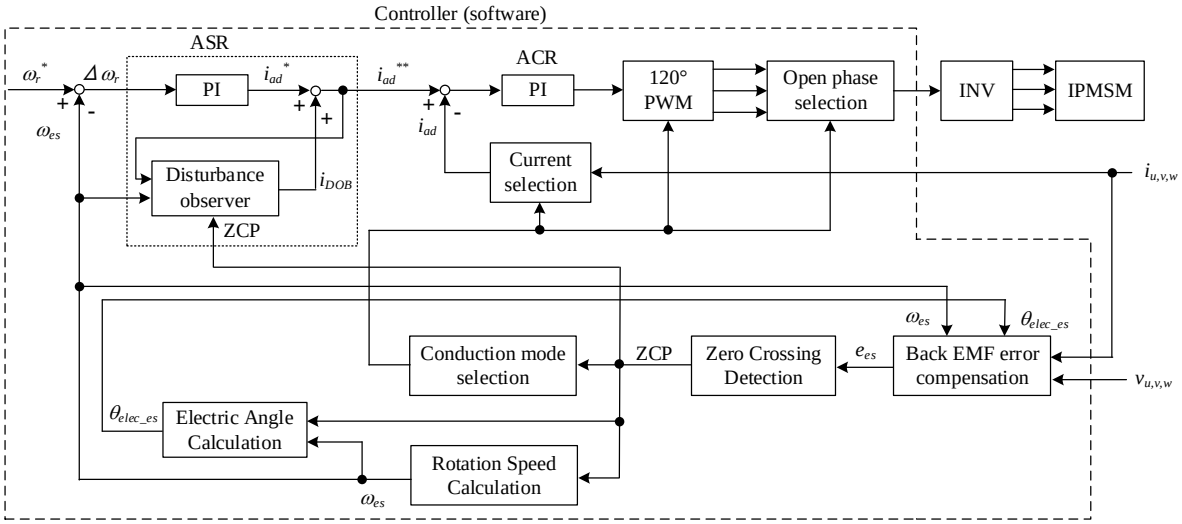

Fig. 3. Motor control configuration for compressor drive.

the conduction phase. The ASR is composed of a PI controller and disturbance observer. The PI controller controls the average speed, while the disturbance observer is implemented to reduce the speed ripple. The rotation speed calculation estimates the average speed from the time interval between ZCPs. As shown in Fig. 4, the ZCPs are obtained by the star-connected resistance on the inverter output.

In the start-up of the motor, an open-loop operation accelerates the motor speed from 0 to 0.125p.u., which enables the controller to detect the back EMF [12]. Then, the control method is switched to the sensorless control. These sequences are omitted in Fig. 3.

D. Compensation method for error voltage added to back EMF

The inductance of the IPMSMs changes with the electrical angle. Thus, an error voltage appears in the detected voltage of the open phase [13]. The error voltage causes a position detection error and an estimated speed error.

Fig. 5 shows the relationship between the detection voltage v_{open} and the U-phase back EMF e_u in the conduction mode 6, defined in Fig. 2. In the sensorless 120-conduction mode of this paper, the back EMF is detected from the potential difference v_{open} between the virtual neutral point and the open phase, as shown in Fig.4. As a result, the error voltage e_{error} is superimposed on the detection voltage v_{open}. The error voltage e_{error} causes position detection errors due to the discrepancy between the ZCPs of v_{open} and e_u.

The relationship between back EMF e_u, e_v, and e_w and the electric angle θ_{elec} is given by (1).

$$\begin{cases} e_u = E\sin\left(\theta_{elec}\right) \\ e_v = E\sin\left(\theta_{elec} - \dfrac{2}{3}\pi\right) \\ e_w = E\sin\left(\theta_{elec} + \dfrac{2}{3}\pi\right) \end{cases}, \tag{1}$$

where E is the amplitude of the back EMF, which is determined by the motor speed and field flux linkage. In the conduction mode 6, the potential difference v_{open_GND} between GND and the U-phase (open phase) terminal is given by (2), and the potential difference v_{ni_GND} between GND and the virtual neutral point is given by (3).

$$v_{open\_GND} = e_u + v_s^{\,open} + \frac{V_{DC}}{2} - \frac{e_v + e_w + v_s^{\,\theta}}{2}, \tag{2}$$

$$v_{ni\_GND} = \frac{V_{DC} + v_{open\_GND}}{3}, \tag{3}$$

where $v_s^{\,open}$ and $v_s^{\,\theta}$ represent an additional voltage component in EMF and that in terminal voltage varied with respect to the electric angle. Here, $v_s^{\,open}$ and $v_s^{\,\theta}$ are given by (4) and (5), respectively.

$$v_s^{\,open} = p\left(L_{uv}\cdot i_v + L_{uw}\cdot i_w\right), \tag{4}$$

$$v_s^{\,\theta} = p\left(L_v\cdot i_v + L_w\cdot i_w\right), \tag{5}$$

where p is the differential operator, L_{uv} is the mutual inductance between the U and V phases, L_{uw} is the mutual

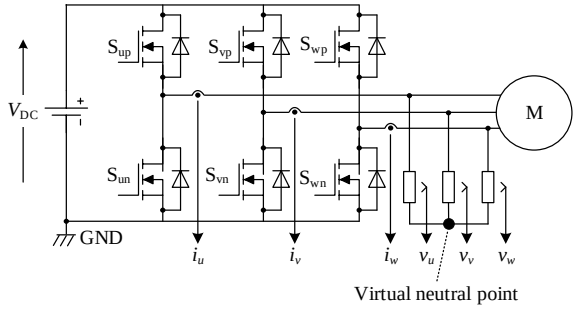

Fig. 4. Circuit configuration of three-phase inverter.

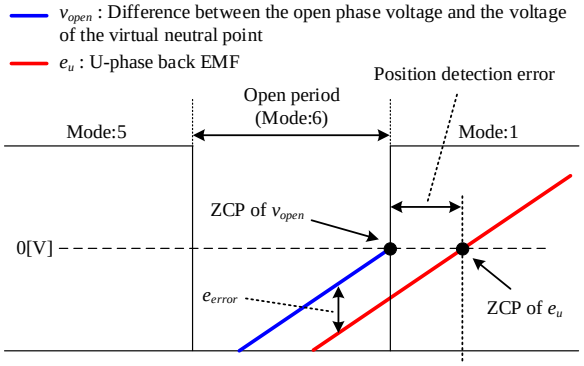

Fig. 5. Conceptual diagram of back EMF error.

inductance between the U and W phases, L_v is the self-inductance of the V-phase, and L_w is the self-inductance of the W-phase. From (1)-(5), v_{open} and e_{error} are given as:

$$v_{open} = v_{open\_GND} - v_{ni\_GND} = e_u + e_{error}, \tag{6}$$

$$e_{error} = \frac{\sqrt{3}}{3}\left(L_q - L_d\right)\left\{2i\omega_{elec}\cos\left(2\theta_{EMF}\right) + pi\cdot\sin\left(2\theta_{EMF}\right)\right\}, \tag{7}$$

where L_d is the d-axis inductance, L_q is the q-axis inductance, ω_{elec} is the electric angular velocity, θ_{EMF} is the angle of the back EMF of the open phase, and i is a current of the two conducting phases, which corresponds to the current flowing to the W and V phases in the conduction mode 6. The error voltage e_{error} is given by (8) as the current derivative term in (7) is simplified to zero.

$$e_{error} = \frac{\sqrt{3}}{3}\left(L_q - L_d\right)\left\{2i\omega_{elec}\cos\left(2\theta_{EMF}\right)\right\}, \tag{8}$$

Eq. (8) reveals that the error voltage e_{error} varies depending on the motor speed, current, and electrical angle.

In order to detect only the back EMF component from the detection voltage v_{open}, it is necessary to subtract the error voltage e_{error} from v_{open}. In this paper, the estimated error voltage e_{error_es} is calculated from the estimated speed and electrical angle obtained by linear interpolation. In this paper, the estimated back EMF is given by subtracting the error voltage component from v_{open} as:

$$e_{error\_es} = \frac{\sqrt{3}}{3}\left(L_q - L_d\right)\left\{2i_{ad}\omega_{elec\_es}\cos\left(2\theta_{EMF}\right)\right\}, \tag{9}$$

$$e_{es} = v_{open} - e_{error\_es}, \tag{10}$$

where ω_{elec_es} is the estimated electric angular velocity, and θ_{EMF_es} is the estimated angle of the back EMF of the open phase obtained in the linear interpolation. The error voltage component is reduced by using (9) and (10).

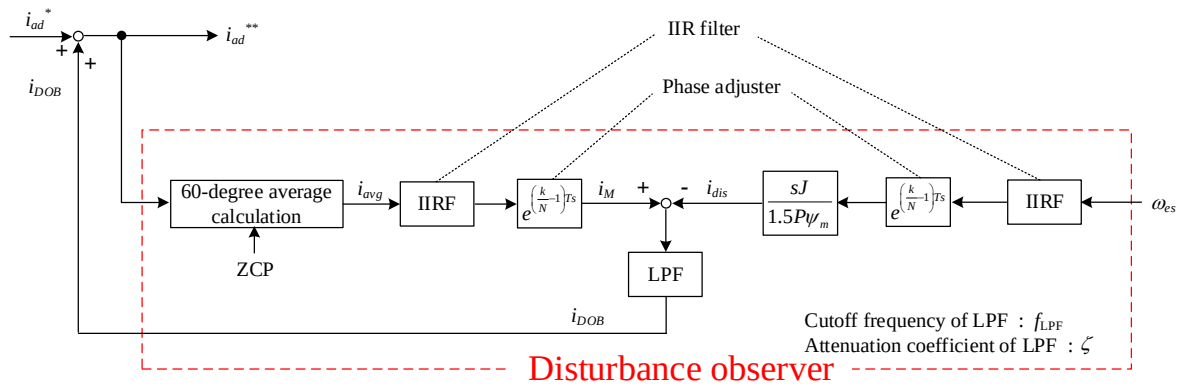

Fig. 6. Control block diagram of proposed disturbance observer.

III. Proposed Vibration Suppression Method

Fig. 6 shows the control block diagram of the proposed disturbance observer. This paper proposes a vibration suppression method using a disturbance observer. The proposed method compensates for the disturbance by using the estimated speed detected at a low speed, which delays due to the coarse sampling. Furthermore, focusing on the periodicity of the load fluctuations, the phase angle of the current command is adjusted to suppress the vibration.

A. Disturbance observer compensated for dead time

Fig. 7(a) shows a simplified control system using the conventional disturbance observer. In Fig. 7(a), i_{ad}^* is the output of the ASR, F is the disturbance, L is the dead time, J is the inertia of the motor, ω is the motor speed, and Q is the transfer function of a low-pass filter (LPF). In the sensorless 120-degree conduction mode, the average speed is estimated from the time interval between ZCPs. Thus, the estimated speed ω_{es} has a dead time L of 60 electrical degrees with respect to the true speed. The characteristic equation of the controller in Fig. 7(a) is given as:

$$\omega = \frac{Ki_{ad}^* + F\left(Q-1\right)}{sJ\left(Qe^{-sL}+1-Q\right)}, \tag{11}$$

The characteristics equation in (11) includes the delay in the denominator. Thus, the stability and disturbance suppression characteristics of the control system deteriorate.

Fig. 7(b) shows the simplified control block diagram of the disturbance observer with the Smith compensator proposed in this paper. The Smith method is one of the dead-time compensation methods [14]. This paper inserts the Smith compensator R at the control input u of the disturbance observer. The compensator R is an identical transfer function with the delay appeared in the detected speed as:

$$R = e^{-sL}, \tag{12}$$

With the compensator R applied, the characteristic equation of the proposed controller in Fig. 7(b) is calculated as (13).

$$\omega = \frac{Ki_{ad}^* + F\left(QR-1\right)}{sJ}, \tag{13}$$

From (13), the compensator R removes the delay from the denominator in the characteristic equation. Therefore, the stability and disturbance suppression characteristics are improved.

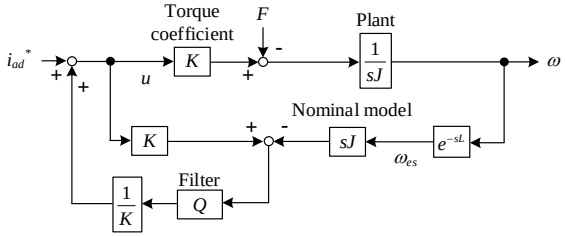

(a). Without compensator.

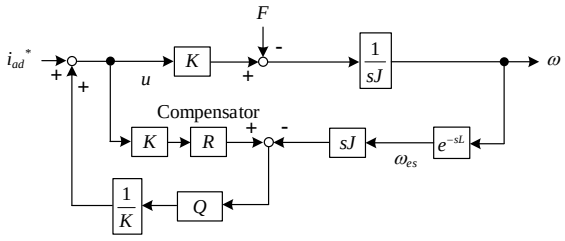

(b). With compensator.

Fig.7. Control system using disturbance observer with Smith's compensator.

Since the average speed during a 60-electrical angle is detected, the Smith compensator of the proposed controller shown in Fig. 6 is an averaging of the current command i_{ad}^{**} during 60-electrical angle, which corresponds to the time interval between two ZCPs. In this paper, a constant torque coefficient is utilized as a plant in the disturbance observer for simplicity, even though i_d is not always zero because of the load fluctuation in the 120-degree conduction mode.

B. Phase correction of current command

In the sensorless 120-degree conduction mode, the estimated speed has a large delay because the motor speed is estimated at the low speed of every 60 electrical degrees. This delay leads to a delay in the compensation current command i_{DOB}, and the vibration suppression effect deteriorates.

In this paper, focusing on the characteristic that the load torque of the compressor fluctuates with the mechanical angular period T, the phase angle of i_{DOB} is compensated. The phase adjuster in Fig. 6 compensates the delay of i_{DOB} by adjusting the constant k to synchronized with the phase

angle of the load torque.

The number of the memories of six times the number of pole pairs P because the phase adjuster is executed only when the ZCP is detected.

C. Improvement of estimated speed resolution using an IIR filter

In the sensorless 120-degree conduction mode, the controller counts the time between two ZCPs in order to obtain the estimated speed. The estimated speed ω_{es} is expressed with the number of counts between two ZCPs as:

$$\omega_{es} = \frac{2\pi}{18T_{sw}n_{60\deg}}, \tag{14}$$

where T_{sw} is the control period of the controller. From (14), the error range of the estimated speed is given by (15).

$$\frac{2\pi}{18T_{sw}\cdot\left\lfloor\frac{2\pi}{18\omega T_{sw}}\right\rfloor} \le \omega_{es} \le \frac{2\pi}{18T_{sw}\left(\left\lfloor\frac{2\pi}{18\omega T_{sw}}\right\rfloor+1\right)}, \tag{15}$$

where ω is the angular velocity of the motor and $\lfloor\square\rfloor$ is the floor function. Fig. 8 shows the relationship between the motor speed and the maximum speed error calculated from (15). From Fig. 8, the resolution of the estimated speed decreases as the motor speed increases, which results in a large error in the compensation current command i_{DOB}. In this paper, an IIR filter is applied to the estimated speed ω_{es} to suppress errors caused by the aforementioned error of the estimated speed.

Fig. 9 shows the control block diagram of the IIR filter applied for the quantization error reduction. Focusing on the periodicity of the load fluctuation, the delay time T in the IIR filter is set to the mechanical angular period. The filter coefficient a is set to 0.95 in order to decrease the effect of quantization error.

In the sensorless 120-degree conduction mode, the estimated speed is calculated based on the electrical angle detected every 60 electrical degrees. This implies that a differential calculation is performed implicitly to obtain the speed from the angle. Therefore, a second-order LPF is adopted in the disturbance observer. In this paper, the cutoff frequency of the LPF is designed to be less than one-third of the detection frequency of the ZCPs. Thus, the main frequency component of the disturbance (load torque) is extracted. The LPF and the Smith compensator also cause a larger delay. Therefore, the constant k in the phase adjuster is designed, taking into account the delay due to the LPF.

D. Stability Analysis Result

Fig. 10 shows the frequency characteristics of the open-loop transfer function of the proposed control system with and without the Smith compensator. The delays in the Smith compensator and estimated speed are set to the period of 60 electrical degrees at a low speed of 15rps (0.19p.u.). The second-order LPF with a cutoff frequency of 80 Hz and an attenuation factor of 1.0 is used. In addition, this analysis assumes the constant torque coefficient of the motor for simplicity. The IIR filter is dropped to confirm the effect of the Smith compensator

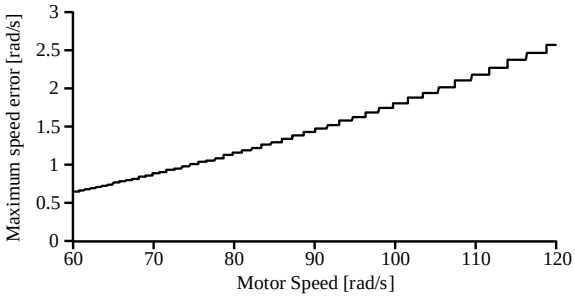

Fig.8. Relationship between true speed and maximum speed error.

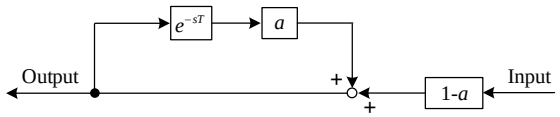

Fig.9. Control block diagram of IIR filter.

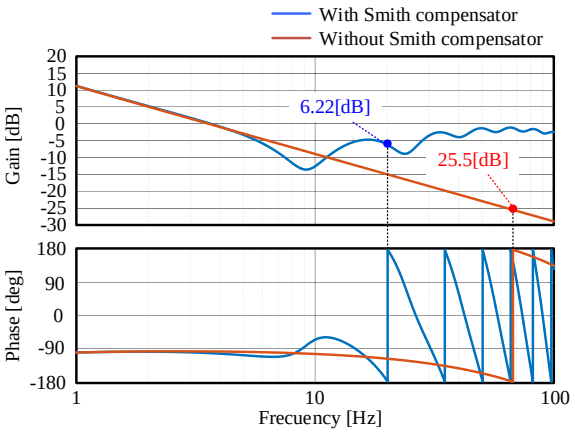

Fig.10. Bode diagram of the proposed control system.

TABLE I
EXPERIMENTAL CONDITIONS

Parameter	Symbol	Value
Rating rotation speed	ω_n	80 rps
Rating torque	T_n	0.237 N・m
Number of pole pairs	P	3
Winding resistance	R	6.2 Ω
d-axis inductace	L_d	76.3 mH
q-axis inductace	L_q	136 mH
Field flux linkage	Ψ_m	0.14 Wb
Inertia moment	J	0.00037 kgm^2
DC-link voltage	V_{dc}	280 V
Switching frequency	f_{sw}	16 kHz
Speed command value	ω_r^*	15 rps
Cutoff frequency of LPF	f_{LPF}	80 Hz
Attenuation coefficient of LPF	ζ	1.0
Phase advance coefficient	k	2
Coefficient of QERF	a	0.95

alone. Fig. 10 shows that the gain margin of the system, which is 6.22dB without the Smith compensator, is improved to 25.5 dB by the Smith compensator. The analysis results clarify that the stability is improved by the Smith compensator.

IV. EXPERIMENTAL RESULTS

Table 1 shows the motor parameters and experimental conditions. The compressor vibration is evaluated at a low speed of 0.19p.u. The compressor vibration is measured using the acceleration sensor (Ono Sokki, NP-3120) and

the sensor amplifier (Ono Sokki, SR-2210, FLAT mode).

Fig. 11 shows the experimental waveforms with and without the proposed disturbance observer. In Fig. 11(a), the motor speed is controlled only by the PI controller. Thus, the speed ripple is not suppressed, and large vibration occurs. On the other hand, in Fig. 11(b), the compensation current command obtained by the proposed disturbance observer fluctuates at the mechanical frequency. As a result, the speed ripple is suppressed to almost zero, and the compressor vibration is also suppressed owing to the disturbance observer.

Fig. 12 shows the harmonic analysis result of the vibration with and without the disturbance observer. The fundamental frequency component of the vibration is reduced by 94.2% when the disturbance observer is applied.

V. Conclusions

This paper proposed the vibration suppression method for a compressor motor driven in the sensorless 120-degree conduction mode. The proposed method focuses on the periodicity of the load and suppresses the vibration by the disturbance observer with the Smith compensator. The experimental results showed that the proposed method reduced the fundamental frequency component of the vibration by 94.2% at the low speed of 0.19p.u. In future work, the robustness of the proposed control system under motor parameter variation will be evaluated.

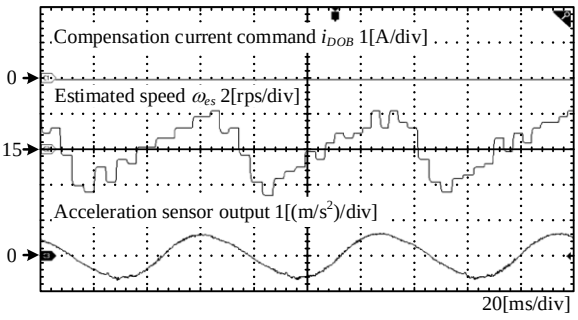

(a). Without applying DOB.

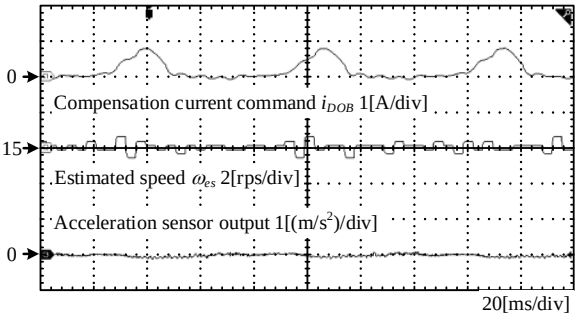

(b). With applying DOB.

Fig.11. Waveforms of compensation current command i_{DOB}, estimated speed ω_{es}, and acceleration sensor output (0.19p.u. speed).

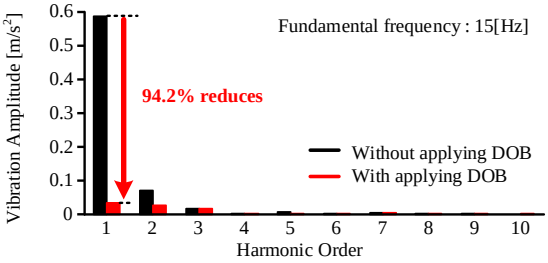

Fig.12. Harmonic analysis results of vibration.

References

[1] S. Morimoto, Y. Inoue, M. Sanada, " Reducing Cogging Torque with Rotor Surface Notches in Double-Layered IPMSMs," IEEJ Journal of Industry Applications, vol. 12, no. 6, pp. 1096-1103 (2023)

[2] S. Sasayama, Y. Shimizu, S. Morimoto, Y. Inoue, M. Sanada, " Maximum Torque per Ampere Control of IPMSM Using Online Flux Linkage Plane Estimation Considering Cross Saturation," IEEJ Journal of Industry Applications, vol. 12, no. 3, pp. 319-325 (2023)

[3] M. Horiuchi, R. Masuda, Y. Bu, M. Nirei, M. Sato, T. Mizuno, " Effect of Magnetic Wedge Characteristics on Torque Ripple and Loss in Interior Permanent Magnet Synchronous Motor," IEEJ Journal of Industry Applications, vol. 11, no. 1, pp. 49-58 (2022)

[4] T. Noguchi, "Trends of permanent-magnet synchronous machine drives," IEEJ Transaction on electrical and electronic engineering, Vol.2, No.2, pp.125-142 (2007)

[5] S. Hattori, "Vibration Suppression Control Method for PMSMs Based on Learning Control Corresponding to Operating Point Changes," IEEJ Transactions on Industry Applications, vol. 137, no. 1, pp. 10-16 (2017)

[6] Y. Notohara, D. Li, Y. Iwaji, M. Tamura, and K. Tsukii, "Study on Vibration Suppression Control for Rotary Compressor," IEEJ Transactions on Industry Applications, vol. 140, no. 11, pp. 841-847 (2020)

[7] Y. Omi, T. Yasuda, T. Kumagai, H. Watanabe and J. Itoh, "Vibration Reduction Method by Instantaneous Current Control in 120-degree Conduction Mode of Compressor Motor," 2023 25th European Conference on Power Electronics and Applications (EPE'23 ECCE Europe), Aalborg, Denmark, pp. 1-9 (2023)

[8] P. Damodharan and K. Vasudevan, "Sensorless Brushless DC Motor Drive Based on the Zero-Crossing Detection of Back Electromotive Force (EMF) From the Line Voltage Difference," IEEE Transactions on Energy Conversion, vol. 25, no. 3, pp. 661-668 (2010)

[9] T.-H. Kim and M. Ehsani, “Sensorless control of BLDC motors from near-zero to high speeds,” IEEE Trans. Power Electron., vol. 19, no. 6, pp. 1635–1645 (2004)

[10] T. Shioi, T. Kumagai, K.Kusaka, and J. Itoh, "Estimation Method of Load Torque Characteristics and Mechanical Parameter for Reciprocating Compressor Considering Pressure variation," IEE-Japan Industry Applications Society Conference, no. 4-4, pp. IV-95 (2021)

[11] C. -L. Chiu, Y. -T. Chen, Y. -H. Shen and R. -H. Liang, "An Accurate Automatic Phase Advance Adjustment of Brushless DC Motor," IEEE Transactions on Magnetics, vol. 45, no. 1, pp. 120-126 (2009)

[12] J. Liu, T. A. Nondahl, J. Dai, S. Royak, and P. B. Schmidt, "Seamless Transition Scheme of Position Sensorless Control in Industrial Permanent Magnet Motor Drives With Output Filter and Transformer for Oil Pump Applications," IEEE Transactions on Industry Applications, vol. 56, no. 3, pp. 2180-2189 (2020)

[13] D. Lee and W. Lee, " Analysis of Relationship Between Abnormal Current and Position Detection Error in

Sensorless Controller for Interior Permanent-Magnet Brushless DC Motors," IEEE TRANSACTIONS ON MAGNETICS, Vol. 44, No. 8, pp.2074-2081 (2008)

[14] R. Hotchi, H. Chibana, T. Iwai and R. Kubo, "Active Queue Management Supporting TCP Flows Using Disturbance Observer and Smith Predictor," IEEE Access, vol. 8, pp. 173401-173413 (2020)